J Arid Land (2025) 17(5): 624–643
doi: 10.1007/s40333-025-0014-x; CSTR: 32276.14.JAL.0250014x

Science Press Springer-Verlag

Variations of soil moisture and its influencing factors in arid and semi-arid areas, China

NIU Jiqiang[1,2*], LIU Zijian[1], CHEN Feiyan[1,2], LIU Gangjun[3], ZHOU Junli[4], ZHOU Peng[5,6], LI Hongrui[1], LI Mengyang[1]

[1] School of Geographic Sciences, Xinyang Normal University, Xinyang 464000, China;
[2] Henan Key Technology Engineering Research Center of Microwave Remote Sensing and Resource Environment Monitoring, Xinyang Normal University, Xinyang 464000, China;
[3] School of Science, STEM College, Royal Melbourne Institute of Technology (RMIT) University, Melbourne 3001, Australia;
[4] Henan Remote Sensing Institute, Zhengzhou 450000, China;
[5] Key Laboratory of Environmental Change and Natural Disaster of Ministry of Education, Beijing Normal University, Beijing 100875, China;
[6] Institute of Disaster Risk Science, Faculty of Geographical Science, Beijing Normal University, Beijing 100875, China

Abstract: Soil moisture (SM) is a critical variable in terrestrial ecosystems, especially in arid and semi-arid areas where water sources are limited. Despite its importance, understanding the spatiotemporal variations and influencing factors of SM in these areas remains insufficient. This study investigated the spatiotemporal variations and influencing factors of SM in arid and semi-arid areas of China by utilizing the extended triple collation (ETC), Mann-Kendall test, Theil-Sen estimator, ridge regression analysis, and other relevant methods. The following findings were obtained: (1) at the pixel scale, the long-term monthly SM data from the European Space Agency Climate Change Initiative (ESA CCI) exhibited the highest correlation coefficient of 0.794 and the lowest root mean square error (RMSE) of 0.014 m^3/m^3; (2) from 2000 to 2022, the study area experienced significant increase in annual average SM, with a rate of 0.408×10^{-3} $m^3/(m^3\cdot a)$. Moreover, higher altitudes showed a notable upward trend, with SM increasing rates at 0.210×10^{-3} $m^3/(m^3\cdot a)$ between 1000 and 2000 m, 0.530×10^{-3} $m^3/(m^3\cdot a)$ between 2000 and 4000 m, and 0.760×10^{-3} $m^3/(m^3\cdot a)$ at altitudes above 4000 m; (3) land surface temperature (LST), root zone soil moisture (RSM) (10–40 cm depth), and normalized difference vegetation index (NDVI) were identified as the primary factors influencing annual average SM, which accounted for 34.37%, 24.16%, and 22.64% relative contributions, respectively; and (4) absolute contribution of LST was more significant in subareas at higher altitudes, with average absolute contributions of 0.800×10^{-3} $m^3/(m^3\cdot a)$ between 2000 and 4000 m and 0.500×10^{-2} $m^3/(m^3\cdot a)$ above 4000 m. This study reveals the spatiotemporal variations and main influencing factors of SM in Chinese arid and semi-arid areas, highlighting the more pronounced absolute contribution of LST to SM in high-altitude areas, providing valuable insights for ecological research and water resource management in these areas.

Keywords: soil moisture; arid and semi-arid areas; remote sensing; extended triple collation; ridge regression analysis

Citation: NIU Jiqiang, LIU Zijian, CHEN Feiyan, LIU Gangjun, ZHOU Junli, ZHOU Peng, LI Hongrui, LI Mengyang. 2025. Variations of soil moisture and its influencing factors in arid and semi-arid areas, China. Journal of Arid Land, 17(5): 624–643. https://doi.org/10.1007/s40333-025-0014-x; https://cstr.cn/32276.14.JAL.0250014x

1 Introduction

Soil moisture (SM) is a crucial variable in the climate system as it regulates plant transpiration

*Corresponding author: NIU Jiqiang (E-mail: niujiqiang@xynu.edu.cn)
Received 2024-09-13; revised 2025-02-16; accepted 2025-03-19

and photosynthesis, thus influencing the cycling of water and energy (Seneviratne et al., 2010). It plays a vital role in climate prediction by controlling the distribution of energy between latent and sensible heat fluxes at the soil-atmosphere interface (Muñoz-Sabater et al., 2012). The availability of soil water is also crucial for maintaining ecological stability (Yang et al., 2014; Zhang et al., 2019). As SM fluctuates, it alters interactions among ecohydrological processes at the land surface (Zhang et al., 2019). The primary methods for SM detection include ground-based measurements and remote sensing techniques, employing both airborne and spaceborne platforms (Peng and Loew, 2017; Zhang et al., 2019). In recent decades, SM monitoring using remote sensing has been deeply researched due to the advancements in Earth observation technology (Seneviratne et al., 2010; Peng and Loew, 2017). Significant progress has been achieved in retrieving SM from microwave observations, resulting in the development of several global SM products (Njoku et al., 2003; Han et al., 2012), including Advanced Microwave Scanning Radiometer-Earth Observing System (AMSR-E) (Owe and de Jeu R Holmes, 2008), the Advanced Scatterometer (ASCAT), the Soil Moisture and Ocean Salinity (SMOS) mission, the Soil Moisture Active Passive (SMAP) (Entekhabi et al., 2010), and the European Space Agency's Climate Change Initiative (ESA CCI) SM products (Wagner et al., 2012; Rahmani et al., 2016). In addition, global SM datasets are provided by systems like Global Land Data Assimilation System (GLDAS) of National Aeronautics and Space Administration (NASA) and the European Centre for Medium-Range Weather Forecasts (ECMWF) Re-Analysis-Interim **(**ERA-Interim) climate reanalysis dataset.

Global SM data are widely utilized in hydrological research (Dorigo et al., 2015; Cai et al., 2017; Wu et al., 2021) and have been validated extensively by scholars using *in situ* observational data (Albergel et al., 2012). *In situ* SM data from over 200 stations across Africa, Australia, Europe, and the United States have been employed to assess the reliability of three SM products, i.e., ECMWF's SM-DAS-2, and the remotely sensed products ASCAT and SMOS. The correlation with *in situ* data was highly satisfactory across most study areas, which encompassed diverse biomes and climatic conditions. Average correlation coefficients were 0.70 for SM-DAS-2, 0.53 for ASCAT, and 0.54 for SMOS (Albergel et al., 2012; Wu et al., 2021). ERA5-Land and GLDAS have also been evaluated for accuracy. ERA5-Land showed a larger bias in semi-humid areas (0.06 m^3/m^3), while GLDAS was generally unbiased. However, GLDAS showed higher temporal precision in northern arid areas, while ERA5-Land performed better in southern humid areas (Dorigo et al., 2012). Furthermore, analysis of ESA CCI, GLDAS-Noah, and ERA-Interim soil moisture data from 1988 to 2010 revealed consistent global drying trends, despite spatial variations in the observed patterns. However, variations in the spatial patterns of these trends underscore the importance of assessing the reliability of SM products. The limitations of *in situ* measurements, such as sparse station coverage and scale mismatches between point-based data and satellite pixels, present challenges for evaluating SM products. Additionally, the short observation periods of station-based SM data make them suitable for validating short-term SM products but insufficient for assessing the reliability of long-term SM time series (Deng et al., 2020a). To address these challenges, researchers used the extended triple collation (ETC) method to evaluate multi-source SM products (Klaus et al., 2010). The ETC method builds on the foundation of the original triple collation (TC) method, a robust, objective, and promising evaluation approach. The TC method can simultaneously estimate the errors of three data sources (Su et al., 2014). However, it is unable to calculate the correlation coefficients between the three datasets and the unknown true SM. In contrast, ETC not only provides error estimates for the each but also calculates the correlation coefficients between the three datasets and the unknown true SM (McColl et al., 2017; Chen et al., 2018).

Previous studies have demonstrated that multiple factors, including precipitation, temperature, and vegetation, influence the spatiotemporal variations in SM (Wang et al., 2013; Cheng and Huang, 2016; Deng et al., 2020a). In areas with limited water availability, SM directly controls evapotranspiration, potentially creating a positive feedback loop with precipitation through moisture recycling (Seneviratne et al., 2010; Zhou et al., 2021). Precipitation serves as a primary

source of SM, and it can directly supplement SM (Wu et al., 2002). With global climate warming, land surface temperatures are rising, which affects SM by altering the land surface energy budget. Increased temperatures lead to higher evapotranspiration rates, thereby reducing SM (Cheng and Huang, 2016). In arid and semi-arid areas with lower altitude, rising surface temperatures exacerbate evapotranspiration, creating a negative feedback mechanism with SM. Conversely, in higher elevation areas, a positive feedback mechanism may emerge between surface temperature and SM. Rising temperatures cause mountain snow and frozen soil to melt, replenishing SM in these areas. Uneven terrain significantly influences the spatial variability of SM, by enhancing its heterogeneity and determining its distribution at the watershed scale. The terrain in Chinese arid and semi-arid areas is particularly complex, with significant elevation differences between adjacent areas, making it necessary to explore SM in different topographic areas. Vegetation is a key variable in alpine ecosystems, where elevation differences can lead to varying conditions for vegetation growth. Vegetation can store and conserve water but can also absorb and deplete SM (Dorigo et al., 2015; Wang et al., 2018b; Zhao, 2021). This dual role contributes to the complex relationship between SM and vegetation. Additionally, there is a strong correlation between surface and deep SM, especially in arid areas, where the relationship often exhibits a negative trend. This phenomenon underscores the need for further investigation into the relationship between deep and surface SM in dryland areas.

Previous studies have investigated changes in SM and its influencing factors. However, utilizing multi-source SM data, research specifically addressing changes in SM and its drivers within arid and semi-arid areas, China remains relatively limited. To address this gap, the aims of the study are: (1) to evaluate three SM products using the ETC method; (2) to select SM product with the best performance to assess SM trends in arid and semi-arid areas of China; (3) to divide the overall study area into four subareas based on SM variations across different altitude zones; and (4) to analyze the main driving factors influencing SM changes in both the overall study area and the subareas.

2 Materials and methods

2.1 Study area

Based on aridity (Allen et al., 1998), researchers classified Chinese climate into four types, i.e., humid, semi-humid, semi-arid, and arid. The aridity index in semi-arid and arid areas is greater than or equal to 1.50. The arid and semi-arid areas of China mainly include eastern Inner Mongolia Autonomous Region, Xinjiang Uygur Autonomous Region, Xizang Autonomous Region, Shanxi, Shaanxi, Gansu provinces, and northern Qinghai Province (Fig. 1).

The study area is located between 25°–47°N and 78°−118°E, covering an area of approximately 4.61×10^6 km^2, which accounts for about 48.00% of Chinese total land area. The arid and semi-arid areas are situated in the interior of China and feature diverse topography, including plateaus, mountains, deserts, and basins. Altitudes range from –185 to 8728 m, with an annual average temperature of 3.80°C. Precipitation is highly variable with an average annual precipitation of less than 400.00 mm. Precipitation is spatially and temporally uneven, combined with high evaporation rates, resulting in frequent drought conditions. Vegetation coverage is relatively sparse, and the ecosystems are fragile, underscoring the importance of analyzing the trends and drivers of SM changes in this area.

2.2 Data sources

2.2.1 SM datasets

The ESA CCI SM product is created by combining SM data from both active and passive microwave sensors (Dorigo et al., 2017). The ESA CCI SM product is composed of three components, i.e., the passive microwave product, which integrates four passive microwave SM datasets using AMSR-E SM as the reference; the active microwave product, which merges two active microwave SM datasets using ASCAT SM as the reference; and the combined product,

which merges both passive and active products (Gruber et al., 2019). Previous research has indicated that, apart from ASCAT, the combined product of ESA CCI outperforms each microwave product it includes (Dorigo et al., 2015). For this study, the combined product from ESA CCI was selected, with the time series covering the period from 2000 to 2022. SM retrieval depth for this product is approximately 5 cm.

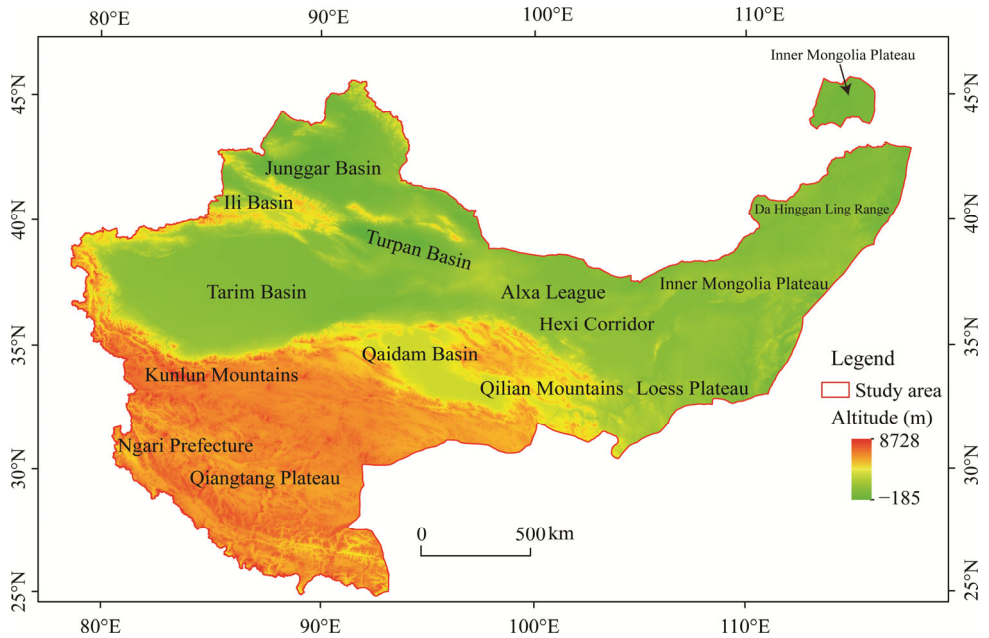

Fig. 1 Geographic location and digital elevation data of the study area. Note that the figure is based on the standard map (No. GS(2019)1822) of the Map Service System (https://bzdt.ch.mnr.gov.cn/), and the boundary has not been modified.

The ERA5-Land SM product is produced by replaying the land component of the ECMWF ERA5 climate reanalysis. Reanalysis combines model data with global observations to create a comprehensive and consistent dataset using the laws of physics (Muñoz-Sabater et al., 2021). The model used in the production of ERA5-Land is the tiled ECMWF Scheme for Surface Exchanges over Land (H-TESSEL), which incorporates land surface hydrology (Wu et al., 2021). The ERA5-Land SM product has undergone significant improvements in time coverage, prediction models, and error correction (Lal et al., 2022). Additionally, the product includes four layers of SM at depths of 0–7, 7–28, 28–100, and 100–289 cm. For this study, the SM data at the depth of 0–7 cm were selected, with a time series spanning from 2000 to 2022.

The GLDAS is a collaborative initiative between NASA's Goddard Space Flight Center and National Centers for Environmental Prediction of the United States National Oceanic and Atmospheric Administration (NOAA). It combines surface observations and satellite remote sensing data to produce SM products by simulating four land surface process models, including the Noah model (Rodell et al., 2004). SM products from the Noah model usually contained four layers of SM data at the depths of 0–10, 10–40, 40–100, and 100–200 cm. For this study, SM data at the depth of 0–10 cm were selected (Zhang et al., 2021), with a time series spanning from 2000 to 2022.

2.2.2 Auxiliary data

Precipitation data were sourced from the Global Precipitation Measurement (GPM), available at NASA's Goddard Space Flight Center. The GPM mission is a global satellite initiative that provides advanced rainfall and snowfall observations every 3 h. Rainfall estimates were derived using the integrated multi-satellite retrievals for the GPM algorithm, which combines data from all passive-microwave instruments in the GPM constellation (Tang et al., 2020). Monthly data

from 2000 to 2022 were accessible via Google Earth Engine (GEE).

Land surface temperature (LST) data and root zone soil moisture (RSM) (10–40 cm) data were sourced from the NASA's Global Land Data Assimilation System 2 (GLDAS-2). GLDAS-2 consists of three components, i.e., GLDAS-2.0, GLDAS-2.1, and GLDAS-2.2. The GLDAS-2.1 component combines model outputs and observational data from 2000 to the present (Han et al., 2020; Luo et al., 2023; Ojha et al., 2024). The dataset selected for this study comes from the GLDAS Noah Land Surface Model.

Evapotranspiration data were obtained from the Global Land Evaporation Amsterdam Model (GLEAM). GLEAM is a set of algorithms designed to estimate various land evaporation contents, such as transpiration, bare-soil evaporation, interception loss, open-water evaporation, and sublimation (Miralles et al., 2011; Liu et al., 2021). GLEAM methodology maximizes the use of satellite-derived climatic and environmental data to estimate evaporation. For this study, monthly evapotranspiration data from 2000 to 2022 were used.

Normalized difference vegetation index (NDVI) data were sourced from the NASA's Land Processes Distributed Active Archive Center. The dataset used in this study is Global MOD13A2 at 1 km spatial resolution (Cheng et al., 2022). NDVI data from 2000 to 2022 ware retrieved using GEE. The basic data information used in this study is shown in Table 1.

Table 1 Basic data information used in this study

Data	Data type	Temporal coverage (yyyy-mm-dd)	Spatial resolution	Temporal resolution
ESA CCI SM	Remote sensing	1978-01-01–Present	0.25°	daily
ERA5-Land SM	Reanalysis	1950-01-01–Present	0.25°	daily/monthly
GLDAS SM	Land model	2000-01-01–Present	0.25°	daily/monthly
Precipitation	Remote sensing	2000-06-01–2024-06-01	0.10°	monthly
LST and RSM	Land model	2000-01-01–2024-03-31	0.25°	monthly
Evapotranspiration	Land model	1980-01-01–2022-12-31	0.10°	monthly
NDVI	Remote sensing	2000-02-18–2024-06-09	1 km	16 d

Note: ESA CCI, European Space Agency's Climate Change Initiative; SM, soil moisture; ERA5-Land, European Centre for Medium-Range Weather Forecasts-Analysis-Land; GLDAS, Global Land Data Assimilation System; LST, land surface temperature; RSM, root soil moisture (10–40 cm); NDVI, normalized difference vegetation index. The abbreviations are the same in the following tables and figures.

2.3 Data analysis

ETC is a method used for estimating errors and correlation coefficients of unknown targets. ETC extends the classical triple collocation (TC) method. The TC method is a statistical approach designed to estimate the variance of random errors in three independent datasets (Zhang et al., 2023b). It assumes a linear relationship between the three SM data products and the true SM. This relationship can be expressed as follows:

$$\mathrm{SM}_i = \mathrm{SM}'_i + \varepsilon_i = \alpha_i + \beta_i S + \varepsilon_i , \tag{1}$$

where SM_i is the actual soil moisture value (m^3/m^3); SM'_i is the soil moisture values from a dataset (m^3/m^3); ε_i is the random errors (m^3/m^3); α_i and β_i are the intercepts and slopes, respectively, which are determined through ordinary least squares (OLS) regression (Stoffelen, 1998; McColl et al., 2014); and S is the true soil moisture value (m^3/m^3).

The covariance between different measurement systems can be expressed as follows:

$$\begin{aligned} &\mathrm{Cov}(\mathrm{SM}_i, \mathrm{SM}_j) = E(\mathrm{SM}_i \mathrm{SM}_j) - E(\mathrm{SM}_i) E(\mathrm{SM}_j) = \\ &\beta_i \beta_j \delta_S{}^2 + \beta_i \mathrm{Cov}(S, \varepsilon_i) + \beta_j \mathrm{Cov}(S, \varepsilon_j) + \mathrm{Cov}(\varepsilon_i, \varepsilon_j) \end{aligned} , \tag{2}$$

where SM_j is the values in different soil moisture datasets (m^3/m^3); E is the expected value; β_j is the slopes; $\delta_S{}^2$ is the variance of the true value S; and ε_j is the random error. The TC method assumes that the random errors in the three input datasets are mutually independent ($\mathrm{Cov}(\varepsilon_i, \varepsilon_j=0)$); the expected values of the random error are zero ($E(\varepsilon_j)=0$); and there is no covariance between the

random error and the unknown true value (Cov(S, ε_j=0)). The covariance (Q_{ij}) between the SM datasets can be expressed as follows:

$$Q_{ij} = \mathrm{Cov}(\mathrm{SM}_i, \mathrm{SM}_j) = \begin{cases} \beta_i \beta_j {\delta_S}^2, i \neq j \\ \beta_i^2 {\delta_S}^2 + {\delta_{\varepsilon_i}}^2, i = j \end{cases}, \tag{3}$$

where ${\delta_{\varepsilon_i}}^2$ is the variance of the dataset residuals. Since there are six unique terms in the 3×3 covariance matrix (Q_{11}, Q_{12}, Q_{13}, Q_{22}, Q_{23}, and Q_{33}), there are six equations but seven unknowns (β_1, β_2, β_3, δ_{ε_1}, δ_{ε_2}, δ_{ε_3}, and δ_S). To address this, we introduced a new variable: θ_i=$\beta_i\delta_S$, where θ_i is the standard deviation of the slope. The formula can be simplified as follows:

$$Q_{ij} = \begin{cases} \theta_i' \theta_j, i \neq j \\ \theta_i^2 + {\delta_{\varepsilon_i}}^2, i = j \end{cases}, \tag{4}$$

where θ_j' is the standard deviation of the slope for another dataset. The six equations can then be used to solve for the six unknowns. The following equation represents the estimation of root mean square error (RMSE) for the three datasets:

$$\delta_{\varepsilon_i} = \begin{bmatrix} \delta_{\varepsilon_1} \\ \delta_{\varepsilon_2} \\ \delta_{\varepsilon_3} \end{bmatrix} = \begin{bmatrix} \sqrt{Q_{11} - \dfrac{Q_{12}Q_{13}}{Q_{23}}} \\ \sqrt{Q_{22} - \dfrac{Q_{12}Q_{23}}{Q_{13}}} \\ \sqrt{Q_{33} - \dfrac{Q_{13}Q_{23}}{Q_{12}}} \end{bmatrix}. \tag{5}$$

Based on the TC method, McColl et al. (2014) proposed an extension known as ETC to estimate the correlation between SM dataset and true SM. An ordinary OLS solution for Equation 1 can be utilized in the following form:

$$\beta_i = \rho_{S,\mathrm{SM}_i} \frac{\sqrt{Q_{ii}}}{\delta_s}, \tag{6}$$

where $\rho_{\mathrm{S,SM}_i}$ is the correlation coefficient between S and SM_i. The key insight of ETC is that from Equation 6, the correlation can be obtained and used to solve for the unknown parameter:

$$\rho_{S,\mathrm{SM}_i} = \pm \begin{bmatrix} \sqrt{\dfrac{Q_{12}Q_{13}}{Q_{11}Q_{23}}} \\ \mathrm{sgn}(Q_{13}Q_{23}) \sqrt{\dfrac{Q_{12}Q_{23}}{Q_{22}Q_{13}}} \\ \mathrm{sgn}(Q_{12}Q_{23}) \sqrt{\dfrac{Q_{13}Q_{23}}{Q_{33}Q_{12}}} \end{bmatrix}. \tag{7}$$

To avoid numerical issues in the error estimation process, the sample for each independent dataset in this study is over 100.

The Mann-Kendall (MK) test is a non-parametric statistical test used to detect trends and change points in time series data (Mann, 1945; Yue et al., 2002). It is often combined with Theil-Sen trend analysis to assess the changing trends (Sen, 1968).

Multiple linear regression can be applied to analyze the impact of environmental factors on SM (Jung et al., 2017). The model can be expressed as follows:

$$\mathrm{SM} = \sum_{j=1}^{p} \eta_j x_j + k, \tag{8}$$

where j is the number of related factors, and j=1, 2, 3, …; p is the number of independent

variables; η_j is the regression coefficient; x_j is the independent variable;, and k is the term. The η_j is calculated using the least square method:

$$\eta_j = (X^T X)^{-1} X^T y, \tag{9}$$

where X^T is the transpose matrix of X; X is the feature matrix of the independent variables; and y is the vector of the dependent variable.

However, in this study, interactions among variables may lead to multicollinearity, which could cause the matrix X^TX to approach zero, making the regression results unstable. To address this issue, we introduced a perturbation term λI of ridge regression (Kang et al., 2018; Zhao et al., 2023) to estimate the coefficient vector b. The perturbation term effectively mitigates multicollinearity, stabilizing the regression results and reducing sensitivity to multicollinearity.

$$\hat{\eta}_{\text{ridge}} = (X^T X + \lambda I)^{-1} X^T y, \tag{10}$$

where $\hat{\eta}_{\text{ridge}}$ is the estimated coefficient of the ridge regression model; and λI is the regularization term.

In this study, ridge regression was used to quantify the relationships of SM with biological and climatic factors. To facilitate the analysis, we normalized each dataset so that variables with different units can be calculated as follows:

$$X_m = \frac{x - \min(x)}{\max(x) - \min(x)}, \tag{11}$$

where X_m is the normalized biological and climatic data; x is the original data of the variable factor; min(x) is the minimum value in the dataset; and max(x) is the maximum value in the dataset. These normalized data are then input into the ridge regression model:

$$Y_m = \sum_{t=1}^{n} \varphi_t x_{tm} + c, \tag{12}$$

where Y_m is the normalized SM; t is the ordinal number of the independent variable; n is the number of independent variables; φ_t is the regression coefficients; x_{tm} is the normalized climatic and biological factors, and c is the bias of the model. The relative and absolute contributions of each factor to SM were subsequently calculated using the ridge regression coefficients and the standardized trends of climatic and biological factors:

$$\begin{aligned} \gamma_{c1} &= \varphi_t \times X_{\text{is\_trend}} \\ \gamma_{nc1} &= \frac{|\gamma_{c1}|}{|\gamma_{c1}| + |\gamma_{c2}| + |\gamma_{c3}| + |\gamma_{c4}| + |\gamma_{c5}|}. \\ \gamma_{ac1} &= \frac{|\gamma_{c1}|}{Y_{n\_\text{trend}}} \times Y_{\text{trend}} \end{aligned} \tag{13}$$

where γ_{c1} is the contribution of a single factor; $X_{\text{is\_trend}}$ is the trend of the independent variable; γ_{nc1} is the normalized dependent variable; γ_{c1}, γ_{c2}, γ_{c3}, γ_{c4}, and γ_{c5} are the values of different dependent variables; γ_{ac1} is the absolute contribution amounts; and Y_{trend} and Y_{n_trend} are the trend of a single dependent variable and the trend of all dependent variables, respectively.

3 Results

3.1 Evaluation of the three SM products

Under the ETC method, the coefficient of determination (R^2) of the three datasets were 0.629, 0.487, and 0.584, respectively. The average RMSE values were 0.014, 0.025, and 0.016 m^3/m^3 (Fig. 2). Among these, the ESA CCI SM product showed the highest R^2 and the lowest RMSE. In contrast, the ERA5-Land SM product had the lowest R^2 and the highest RMSE. The GLDAS SM product demonstrated a relatively high R^2 and a low RMSE. Therefore, the ESA CCI and GLDAS datasets were more effective at capturing the spatial and temporal variations of surface SM in the study area.

The ETC results showed that ESA CCI generally correlated well with measured data, reflecting the actual conditions in northern China to a large extent. ESA CCI was a remote sensing retrieval dataset that contained missing values due to factors such as clouds, snow, frozen soil, or other influences during data acquisition. For example, the permafrost layer in the western Tibetan Plateau significantly affected ESA's SM retrieval, leading to many missing values.

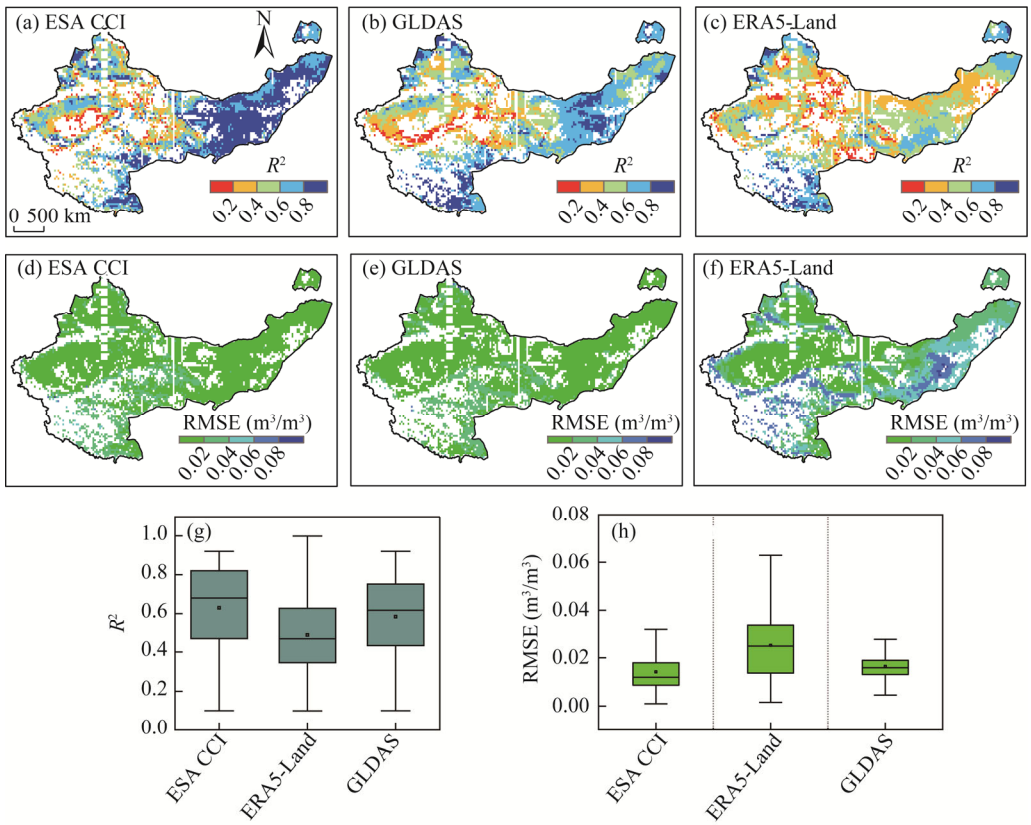

Fig. 2 Coefficient of determination (R^2) and root mean square error (RMSE) of SM data products with unknown true SM. (a and b), ESA CCI; (c and d), GLDAS; (e and f), ERA5-Land; (g and h), the box plot represents R^2 and RMSE of the three datasets against the true SM. Box boundaries indicate the 25th and 75th percentiles, and whiskers below and above the box indicate the 10th and 90th percentiles, respectively. The lines across the boxes indicate the median values, and the points represent the mean values. Blank areas indicate no data or unsatisfied extended triple collation (ETC) condition.

3.2 Trend characteristics of SM

3.2.1 Inter-annual SM dynamics and spatial distribution.

Average annual SM in the study area from 2000 to 2022 ranged from 0.146 to 0.161 m^3/m^3, with an overall average of 0.153 m^3/m^3. Average annual SM exhibited an increasing trend over this period. From 2000 to 2012, the trend was relatively stable, gradually approaching the multi-year average, with a growth rate of 0.660×10^{-3} $m^3/(m^3\cdot a)$. From 2013 to 2017, the average annual SM was higher than the multi-year average, with a growth rate of 0.100×10^{-2} $m^3/(m^3\cdot a)$. From 2018 to 2022, the growth rate reached 0.230×10^{-2} $m^3/(m^3\cdot a)$, which was significantly higher than the previous two periods. According to the MK trend test, the average SM in the study area was estimated to have a Theil-Sen slope of 0.390×10^{-3} $m^3/(m^3\cdot a)$ (Fig. 3).

Regional differences were evident in the spatial distribution of SM trend identified by the MK test. Areas with an increase in SM accounted for 67.13% of the total area, indicating a predominant moist trend across the areas from 2000 to 2022 (Fig. 4). Additionally, 42.62% of the study area experienced a significant increase in SM, primarily in areas such as the Ngari

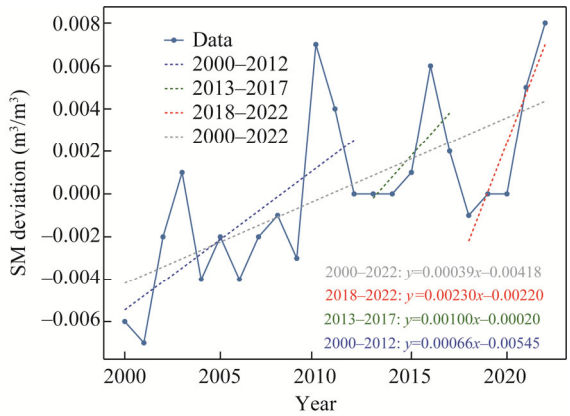

Fig. 3 Linear trend of mean SM in arid and semi-arid areas, China from 2000 to 2022

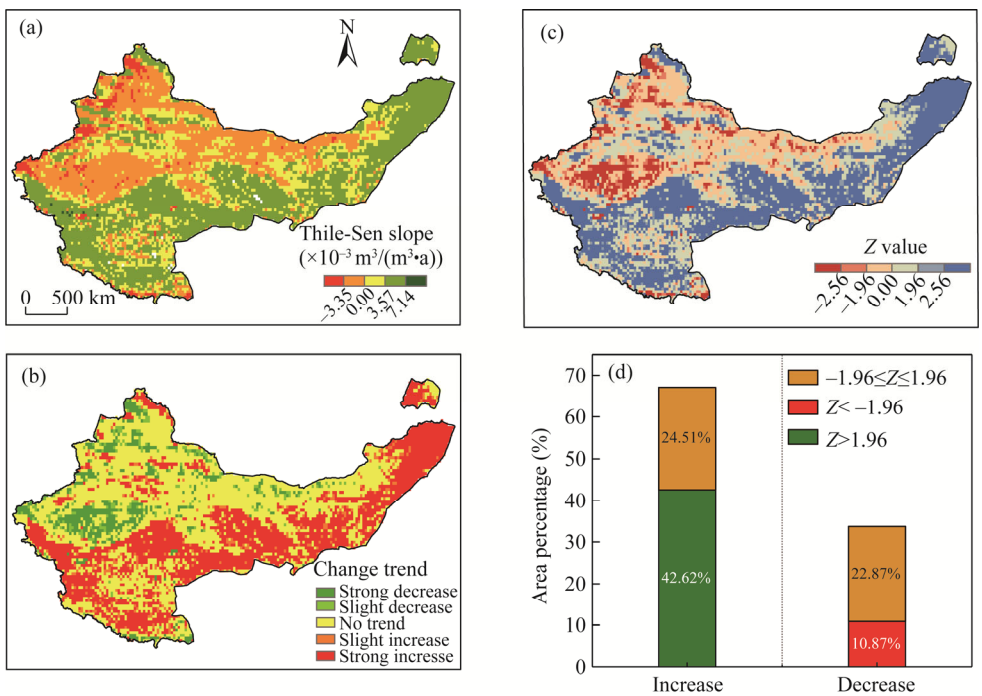

Fig. 4 Trend characteristics of SM in arid and semi-arid areas, China from 2000 to 2022. (a and b), spatial distributions of Theil-Sen slope and its re-classification; (c and d), spatial distribution and its statistics of the Mann-Kendall test. *Z* value is the standardized value of test statistic, and an absolute value greater than 1.96 indicates a significant trend.

Prefecture, Kunlun Mountains, Qiangtang Plateau, Qilian Mountains, northern Loess Plateau, eastern Inner Mongolia Plateau, and southern Da Hinggan Ling Range. Conversely, 10.87% of the study area showed a significant decrease in SM, mainly in the Junggar Basin, Ili Basin, Tarim Basin, and Turpan Basin.

3.2.2 SM trends in different altitudes

The study area displays considerable terrain variation, with substantial altitude differences between adjacent areas. To investigate SM trends across different altitude areas, we resampled the altitude data for the study area to a resolution of 0.25°. The altitude was divided into four levels, i.e., above 4000 m (higher), 2000–4000 m (high), 1000–2000 m (low), and below 1000 m (lower).

The multi-year average SM values for the higher, high, low, and lower altitude areas in the

study area were 0.150, 0.164, 0.146, and 0.145 m^3/m^3, respectively. From 2000 to 2022, three of the four altitude areas exhibited an increasing trend in annual average SM, with the exception of the lower area (Fig. 5).

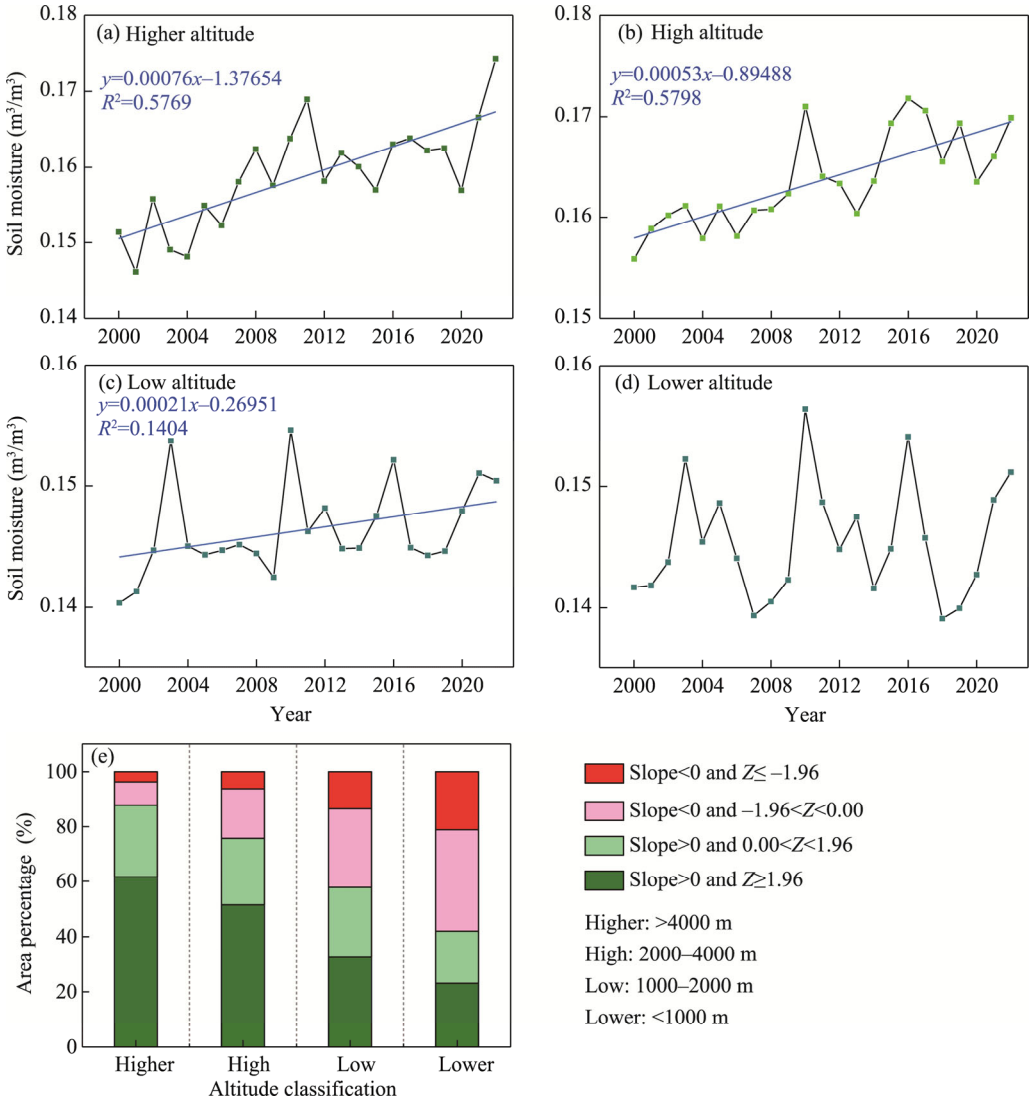

Fig. 5 Average SM trends in different altitude areas from 2000 to 2022. (a), higher altitude area; (b), high altitude area; (c), low altitude area; (d), lower altitude area; (e), statistical results of the Mann-Kendall test.

The higher altitude area exhibited the highest growth rate of 0.760×10^{-3} $m^3/(m^3\cdot a)$, followed by the high and low altitude areas. In contrast, the lower altitude area experienced significant fluctuations in annual average SM without a clear trend over the study period. In the three altitude areas (higher, high, and low areas), the growth rate of annual average SM tended to increase with altitude. The rise in SM of plateau area is likely due to climate warming, which leads to the melting of highland snow or permafrost in the higher altitude areas, replenishing SM and resulting in higher SM values.

3.3 Variability in annual SM

Figure 6 illustrated the spatial patterns and trends of key influencing factors of SM in arid and semi-arid areas from 2000 to 2022, including precipitation, LST, evaporation, NDVI, and RSM.

In the study area, the multi-year average precipitation was 208.73 mm. During the study period,

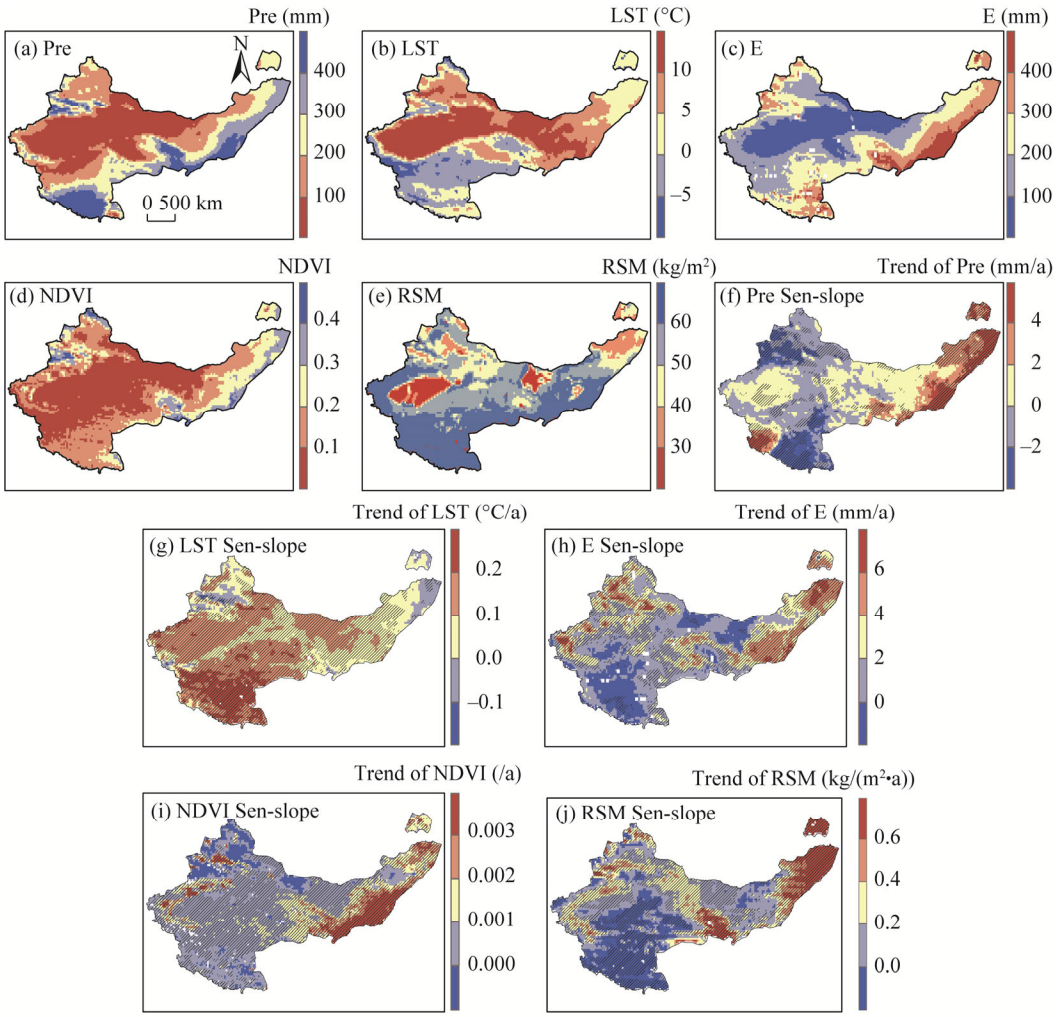

Fig. 6 Spatial patterns (a–e) and trends (f–j) of precipitation (Pre), land surface temperature (LST), evaporation (E), NDVI, and root zone soil moisture (RSM) in arid and semi-arid areas, China from 2000 to 2022

only a small portion of the area (37.57%) showed significant changes. Among these, 20.11% experienced a significant increase, while 17.46% showed a significant decrease. LST exhibited a significant upward trend (0.13°C/a), with 80.91% of the area showing a significant increase and only 1.74% exhibiting a significant decrease. Altitude followed a pattern similar to LST, with a significant overall increase (3.02 mm/a). The majority of the area (52.60%) showed a significant increase, while only 1.95% showed a significant decrease. NDVI showed an upward growth rate of 0.001/a, with 73.41% of the area experiencing a significant increase. RSM also demonstrated an overall upward trend of 0.219 mm/(m^2·a), with 48.94% of the area exhibiting a significant increase and 18.35% showing a significant downward trend. In the study area, the five factors all showed an upward trend, exerting either a promoting or inhibiting effect on SM, and collectively influencing the variations in SM.

Among them, LST had the highest relative contribution to SM, accounting for 34.37%, followed by RSM (24.16%) and NDVI (22.64%). Precipitation had the lowest relative contribution at 8.04% (Fig. 7).

Spatial distribution of SM and driving factors in the study area exhibited significant heterogeneity. Figure 8 shows the spatial patterns of key factors influencing SM trends at each pixel. Specifically, LST had the dominant influence on annual mean SM variation across areas such as western Inner Mongolia Plateau, Alxa League, Hexi Corridor, Tarim Basin, and

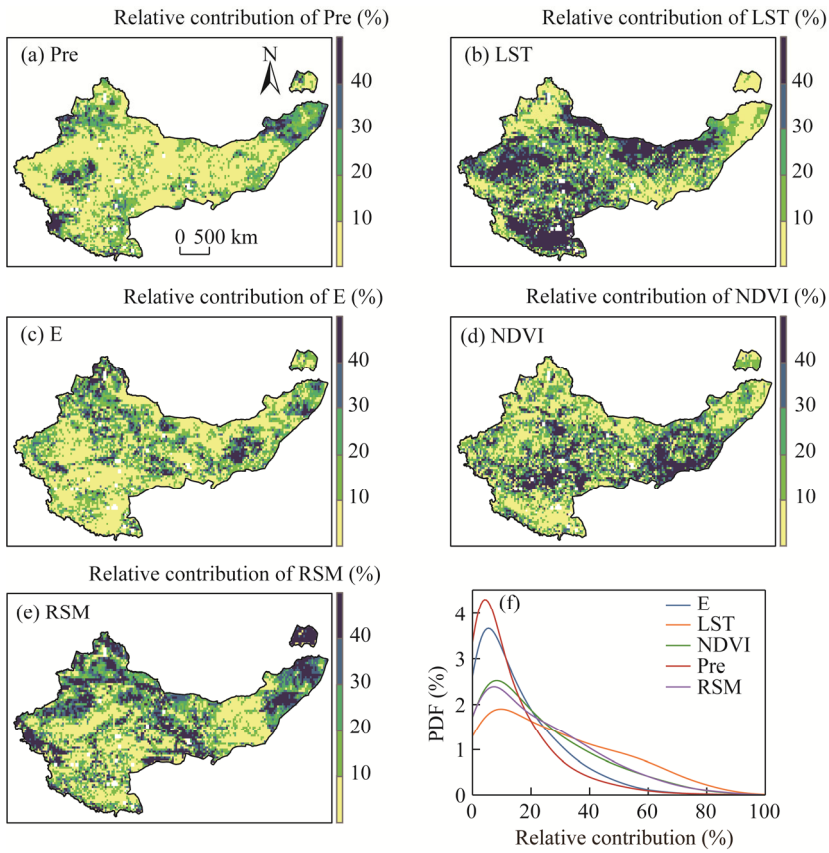

Fig. 7 Relative contributions of Pre (a), LST (b), E (c), NDVI (d), and RSM (e) to annual SM in arid and semi-arid areas, China from 2000 to 2022, and probability density function (PDF) of relative contribution of the five factors (f)

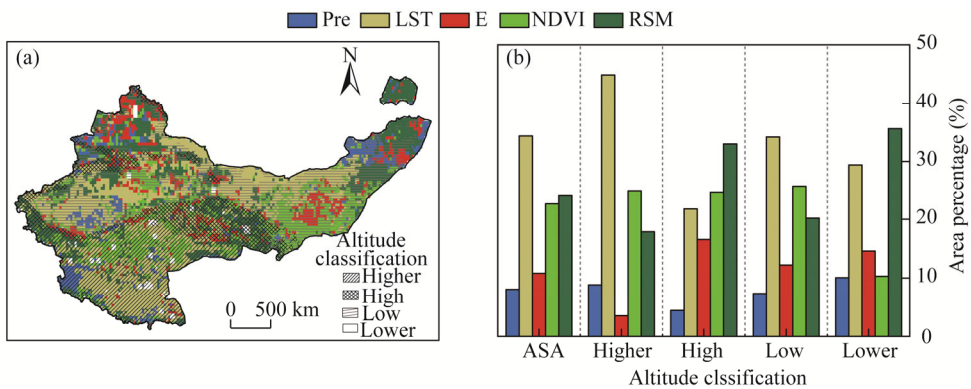

Fig. 8 Spatial distribution (a) and area percentage (b) of dominant factors with the largest relative contribution to annual SM variations across different altitude areas from 2000 to 2022. ASA, arid and semi-arid areas of China.

Qiangtang Plateau. The following significant factors were RSM and NDVI. RSM mainly influenced SM variation in southern Da Hinggan Ling Range, eastern Inner Mongolia Plateau, the Junggar Basin, and northwestern Kunlun Mountains. In the Loess Plateau, NDVI and evaporation were the primary drivers for SM variation. Precipitation had a relatively small and scattered influence on SM variation across the study area. Additionally, the dominant influencing factors varied across the four altitude areas. In the higher altitude area, LST was the first factor that affected annual mean SM variation, followed by NDVI and RSM. RSM had the highest relative

contribution to SM variation in the high altitude area, while NDVI exhibited the highest relative contribution in the low altitude area.

This study systematically investigated the relationships of precipitation, LST, evaporation, and NDVI with RSM at annual-scale variability in SM across the study area. The individual absolute contributions of these factors were also quantified (Fig. 9). Precipitation demonstrated a positive contribution to SM across the entire study area. Combined with Figure 7, this result could be attributed to the reason that the increase in precipitation promoted the rise of SM. LST exhibited the largest absolute contribution to SM in the higher altitude areas. LST promoted the melting of snow or permafrost in high altitude areas, thereby replenishing SM. However, in low altitude areas, the increase in LST led to enhanced evapotranspiration, resulting in a negative contribution to SM. The average absolute contribution of evapotranspiration was negative, but this value was very small, indicating a negative correlation with SM within the study area. NDVI and RSM both exhibited positive contributions in high altitude areas, while their contributions were negative in low altitude areas. The vegetation in low altitude areas was relatively abundant, requiring more RSM, which in turn affected the surface SM.

4 Discussion

4.1 Trends in annual average SM

Approximately 10.00% of global areas exhibit a significant increasing trend in SM, primarily in India, Bangladesh, South Asia, East Africa, and northwestern South America (Deng et al., 2020a). These areas are typically characterized by higher altitudes and are mostly located in arid and semi-arid areas (Zhao and Shi, 2022). In this study, arid and semi-arid areas in China experienced an upward trend in SM from 2000 to 2022 (Fig. 2), aligning with these findings (Tian et al., 2022; Zhao and Shi, 2022).

From 1981 to 2018, SM deficit in most arid areas of northern China exhibited a decreasing trend, showing a temporal trend from wet to dry before 2000, and from dry to wetter from 2000 to 2018 (Xu et al., 2023). From 2000 to 2022, SM in arid and semi-arid areas of China showed a significant upward trend, with the rate of increase gradually accelerating (Fig. 2). SM in northwestern China was generally quite dry, but from 1991 to 2016, SM exhibited an upward trend (Yao et al., 2021). Since the 1990s, SM in the Xizang Plateau exhibited a trend of increased wetness, and with climate warming, precipitation and evapotranspiration also increased (Fang et al., 2021). During the study period, the rate of increase in LST was significant (Fig. 6b), and precipitation and evapotranspiration also showed an upward trend. The rise in LST could have promoted the melting of snow or permafrost, while precipitation and evapotranspiration exhibited a positive feedback mechanism that could accelerate the cycling of water resources, thereby affecting the changes in SM (Cheng and Huang, 2016).

Fang et al. (2021) investigated the response of soil temperature and SM on the Xizang Plateau to climate changes from 1916 to 2010, and found that soil warming began around 1990, followed by an increase after 2000, indicating a general trend of initial warming followed by moistening. Most areas of the study showed a significant upward trend in LST, particularly with a faster rate of increase in higher altitude areas (Fig. 6g). Zhang et al. (2024) used geographic detectors and geographically weighted regression models to analyze the variation trends and driving mechanisms of LST in the Xinjiang Uygur Autonomous Region and found a warming rate of 0.24°C/10 a from 2000 to 2020. Most areas of Xinjiang exhibited an upward trend in LST (Fig. 6g), with an average rate of increase of approximately 0.02°C/10a. Huang et al. (2022) studied the spatial and temporal changes in typical glaciers in northwestern China and their response to climate. From 1990 to 2015, glacier areas decreased by 966.3 km^2, with a correlation coefficient of –0.72 between glacier area and annual average temperature. With global climate warming, LST has shown a significant upward trend over the past two decades (Zhao et al., 2020). Wu et al. (2020) found that East Asia has experienced the fastest temperature increase in Northern Hemisphere

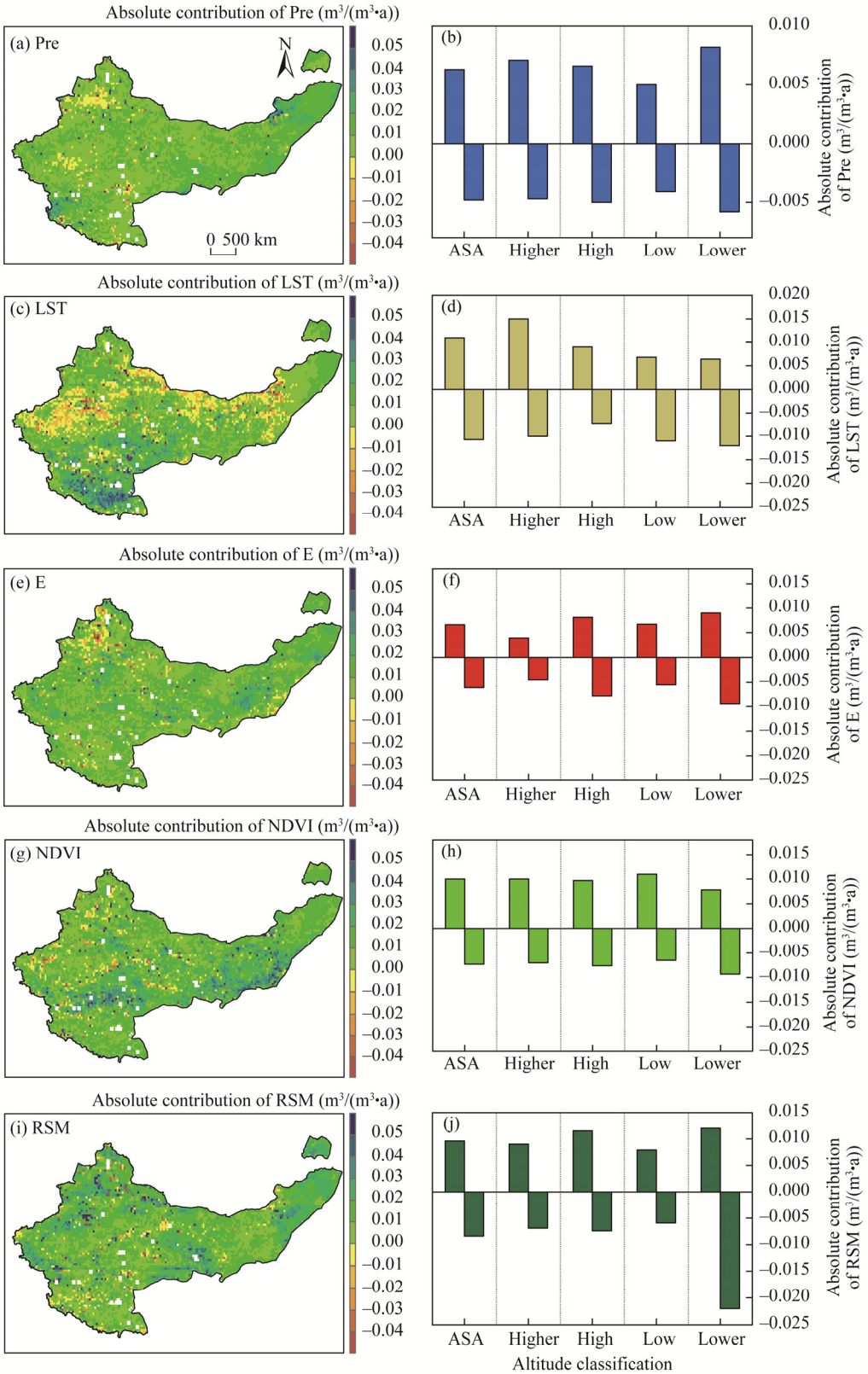

Fig. 9 Spatial distribution and statistics of absolute contribution of five factors to SM in arid and semi-arid areas, China from 2000 to 2022. (a and b), Pre; (c and d), LST; (e and f), E; (g and h), NDVI; (i and j), RSM.

under global warming, accelerating the loss of snow cover in spring and summer. Melting snow, glaciers, and permafrost in high altitude areas have contributed to the increase in SM (Zhu et al., 2022). In this study, the plateau area was characterized by large amounts of snow and permafrost, experiencing melting directly driven by surface temperature, which replenished SM (Meng et al., 2019). LST relative contribution to SM was greater than 30.00% in the plateau area (Fig. 7b). Figure 9 shows the absolute contributions of the five factors to SM. From Figure 9d, the average absolute contribution of LST in high altitude areas was greater than zero, indicating that LST played a significant role in promoting the rise of SM.

4.2 Factors affecting SM

Precipitation is a direct source of SM, and surface SM is highly responsive to changes in precipitation (Lin et al., 2023). Average absolute contribution of precipitation was consistently positive across the entire study area and its subareas (Fig. 9a). This result indicated that during the study period, precipitation was positively correlated with SM, supporting previous researches (Deng et al., 2020a; Lal et al., 2023). Absolute contribution of precipitation was higher in low altitude areas compared with high altitude areas. This disparity may be attributed to the relatively abundant rainfall patterns in low altitude areas, which enable consistent replenishment of SM (Guo et al., 2023). As shown in Figure 6a and f, areas with higher precipitation were primarily located in low altitude areas, where annual average precipitation showed an upward trend during the study period. Therefore, absolute contribution of precipitation to SM was significant in low altitude areas.

As shown in Figure 6d and i, while NDVI was relatively low in arid and semi-arid areas, there was a significant upward trend from 2000 to 2022. The relationship between NDVI and SM remained unclear. Deng et al. (2020b) analyzed the impacts of climate and vegetation changes on SM variations, revealing that vegetation greening exacerbated soil drying. Feng et al. (2016) suggested that vegetation greening increases evapotranspiration in semi-arid areas, leading to excessive SM depletion. For example, excessive vegetation accumulation in the Loess Plateau has been found to cause soil drying (Zhang et al., 2018). In Figure 9g, areas below 1000 m in altitude had relatively rich vegetation, with a higher NDVI, and absolute contribution to SM was negative. However, Li et al. (2018) found that in arid areas, vegetation might have had a positive effect on SM. Positive feedback from vegetation on precipitation could have promoted SM by increasing soil water content. Vegetation regulates the moisture loss to the atmosphere, and increased vegetation can provide shade, reducing soil evaporation (Villegas et al., 2010). Enhanced transpiration from vegetation can also alter precipitation patterns, promoting SM at the regional level (Piao et al., 2019).

The relationship between NDVI and SM is complex and exhibits a bidirectional influence (Li et al., 2024). A threshold exists in the interaction between NDVI and SM, i.e., when NDVI exceeds this threshold, it suppresses SM, while when NDVI is below the threshold, SM promotes the increase in NDVI (Miao et al., 2024). In this study, absolute contribution of NDVI to SM in the higher, high, and low altitude areas was positive, suggesting that NDVI contributed to increasing SM in these areas. However, in the lower altitude area, absolute contribution was negative. This negative contribution may be attributed to the relatively abundant vegetation in the lower altitude areas, where NDVI surpasses the threshold, thereby exerting a suppressive effect on SM (Miao et al., 2024). Zhang et al. (2023a) investigated the determinants of grassland greenness changes in Inner Mongolia Autonomous Region from 1982 to 2016 and found that precipitation and SM accounted for 33.00% and 27.00% of the NDVI variation, respectively. Absolute contribution of NDVI in these altitude areas confirmed its role in promoting SM increases (Fig. 9h).

Evaporation was closely related to temperature and precipitation, with increases in promoting higher rates of evaporation, thereby affecting SM (Li et al., 2013). Evaporation serves as an important intermediary between precipitation and SM, reflecting their interdependent relationship (Gaona et al., 2022). Absolute contributions of evapotranspiration and LST to SM exhibited the

same spatial distribution characteristics (Fig. 9c and e), indicating that the relationship between evapotranspiration and LST was closer within the study area. In arid and semi-arid areas, where annual precipitation ranges from 200.00 to 400.00 mm (Xu et al., 2020), and the annual average temperature is approximately 3.00°C. Absolute contribution of evaporation across the study area was negative, albeit negligible, indicating a weak negative correlation between evaporation and annual SM.

Absolute contribution of RSM across the study area was positive but minimal. Analysis of different altitude areas showed that absolute contribution of RSM was positive in the higher, high, and low altitude areas, but was negative in the lower altitude area, which could be attributed to the relatively abundant vegetation in this area, as vegetation was closely linked to RSM (Li et al., 2024; Miao et al., 2024). Greater vegetation density increases RSM demand, potentially reducing available SM in root zone and indirectly influencing surface SM.

In this study, we applied ridge regression to analyze the impact of climate and environmental variables on SM, conducting the analysis on a pixel-by-pixel basis using annual average values. The contributions of these variables are evaluated for each pixel, with positive values indicating a positive influence and vice versa. Absolute contributions are calculated to capture the interaction between multiple factors, which causes the same factor to have different effects across various areas. For instance, in the high altitude areas, an increase in LST promoted the melting of snow and frozen soil. Due to the relatively low maximum temperature, the increase in evaporation was minimal, resulting in a positive contribution from LST. In contrast, in the low altitude areas, the higher maximum temperature significantly enhanced evaporation, leading to a negative contribution. Precipitation generally showed positive contributions in areas with stable precipitation and minor changes in LST. However, precipitation exhibited negative contributions in areas that experienced decreasing precipitation and rising LST. In sparsely vegetated areas, RSM was minimally consumed. With increased LST, RSM replenished surface SM, leading to positive contributions. In contrast, in areas with abundant vegetation, RSM was consumed extensively by vegetation, resulting in negative contributions in the low altitude area.

4.3 Uncertainty analysis

Three SM datasets used in this study, each with a resolution of 0.25°, generally reflect the spatial characteristics of SM (Ma et al., 2019; Zhu et al., 2019). The ESA CCI SM dataset offers the most accurate result of spatial distribution of actual SM values. However, satellite observation conditions result in discontinuous data, making it unsuitable for long-term time series analysis in the study area. The GLDAS SM dataset performs well in forest, sparse grassland, and agricultural lands, but tends to underestimate actual SM values. Similarly, the ERA5-Land SM dataset shows the highest correlation with real SM in eastern China, but exhibits a consistent underestimation, with the greatest deviation observed in the study area (Hu et al., 2020; Mao et al., 2022). To address these limitations, we used the GLDAS SM dataset to fill gaps in the ESA CCI dataset, enabling the analysis of long-term temporal changes in SM. Although this approach captures overall temporal variation accurately, minor numerical discrepancies relative to actual SM values may exist. SM exhibits significant spatial heterogeneity, with distinct variation patterns across different land use types. Thus, type of classification of the study area is important (Wang et al., 2013; Wang et al., 2018a). Other types of classification such as land use types, watershed types, and vegetation types should be concluded in future researches.

5 Conclusions

This study evaluated spatial and temporal variations of SM in arid and semi-arid areas of China and the main factors driving these variations. Results showed a significant upward trend in SM from 2000 to 2022, particularly in the higher altitude areas, where the increase in SM was more pronounced. The study identified LST, RSM, and NDVI as the main factors influencing SM

variability, with LST having the most substantial impact, especially in the high altitude areas. These findings suggest that climate change, characterized by rising temperatures, is playing a significant role in altering SM dynamics, with the effects differing by altitudes. Future research should focus on long-term monitoring of SM dynamics in relation to vegetation changes and their potential feedback mechanisms in various ecosystems. Additionally, it is crucial to investigate the interplay between surface and RSM across different biomes and their roles in improving predictions of drought conditions under future climate scenarios.

Conflict of interest

The authors declare that they have no known competing financial interests or personal relationships that could have appeared to influence the work reported in this paper.

Acknowledgements

This research was supported by the Natural Science Foundation of Henan Province (252300421290), the National Natural Science Foundation of China (41771438), the Program for Innovative Research Team (in Science and Technology) of Henan University (22IRTSTHN010), and the Postgraduate Education Reform and Quality Improvement Project of Henan Province (HNYJS2020JD14).

Author contributions

Conceptualization: NIU Jiqiang, LIU Zijian; Methodology: LIU Zijian; Software: NIU Jiqiang, ZHOU Junli; validation: LI Hongyrui, LI Mengyang; Formal analysis: CHEN Feiyan; Investigation: LIU Zijian; Resources: NIU Jiqiang; Data curation: LIU Zijian; Writing - original draft preparation: LIU Zijian; Writing - review and editing: LIU Gangjun, ZHOU Peng; Visualization: LI Mengyang; Supervision: CHEN Feiyan; Project administration: NIU Jiqiang; Funding acquisition: NIU Jiqiang. All authors approved the manuscript.

References

Albergel C, Rosnay P, Gruhier C, et al. 2012. Evaluation of remotely sensed and modelled soil moisture products using global ground-based *in situ* observations. Remote Sensing of Environment, 118: 215–226.

Allen R G, Pereira L S, Raes D, et al. 1998. Crop evapotranspiration-guidelines for computing crop water requirements. Food and Agriculture Organization of the United Nations, Rome, 56.

Cai J Z, Zhang Y Z, Li Y, et al. 2017. Analyzing the characteristics of soil moisture using GLDAS Data: A case study in eastern China. Applied Sciences, 7(6): 566, doi: 10.3390/app7060566.

Chen F, Crow W T, Bindlish R, et al. 2018. Global-scale evaluation of SMAP, SMOS and ASCAT soil moisture products using triple collocation. Remote Sensing of Environment, 214: 1–13.

Cheng S J, Huang J P. 2016. Enhanced soil moisture drying in transitional regions under a warming climate. Journal of Geophysical Research: Atmospheres, 121(6): 2542–2555.

Cheng Y, Zhang L J, Zhang Z Q, et al. 2022. Spatiotemporal variation and influence factors of vegetation cover in the Yellow River basin (1982–2021) based on GIMMS NDVI and MOD13A1. Water, 14(20): 3274, doi: 10.3390/w14203274.

Deng Y H, Wang S J, Bai X Y, et al. 2020a. Variation trend of global soil moisture and its cause analysis. Ecological Indicators, 110(10): 105939, doi: 10.1016/j.ecolind.2019.105939.

Deng Y H, Wang S J, Bai X Y, et al. 2020b. Vegetation greening intensified soil drying in some semi-arid and arid areas of the world. Agricultural and Forest Meteorology, 292–293: 108103, doi: 10.1016/j.agrformet.2020.108103.

Dorigo W, Jeu R, Chung D, et al. 2012. Evaluating global trends (1988–2010) in harmonized multi-satellite surface soil moisture. Geophysical Research Letters, 39(18): 52988, doi: 10.1029/2012gl052988.

Dorigo W, Wagner W, Albergel C, et al. 2017. ESA CCI soil moisture for improved Earth system understanding: State-of-the art and future directions. Remote Sensing of Environment, 203: 185–215.

Dorigo W A, Gruber A, De Jeu R A M, et al. 2015. Evaluation of the ESA CCI soil moisture product using ground-based observations. Remote Sensing of Environment, 162: 380–395.

Entekhabi D, Njoku E G, O'Neill P E, et al. 2010. The soil moisture active passive (SMAP) mission. Proceedings of the IEEE, 98(5): 704–716.

Fang X W, Luo S Q, Lyu S H, et al. 2021. Numerical modeling of the responses of soil temperature and soil moisture to climate

change over the Tibetan Plateau, 1961–2010. International Journal of Climatology, 41(8): 4134–4150.

Feng X M, Fu B J, Piao S L, et al. 2016. Revegetation in China's Loess Plateau is approaching sustainable water resource limits. Nature Climate Change, 6(11): 1019–1022.

Gaona J, Quintana-Seguí P, Escorihuela M J, et al. 2022. Interactions between precipitation, evapotranspiration and soil-moisture-based indices to characterize drought with high-resolution remote sensing and land-surface model data. Natural Hazards and Earth System Sciences, 22(10): 3461–3485.

Gruber A, Scanlon T, van der Schalie R, et al. 2019. Evolution of the ESA CCI soil moisture climate data records and their underlying merging methodology. Earth System Science Data, 11(2): 717–739.

Guo W W, Huang S Z, Huang Q, et al. 2023. Precipitation and vegetation transpiration variations dominate the dynamics of agricultural drought characteristics in China. Science of the Total Environment, 898: 165480, doi: 10.1016/j.scitotenv.2023.165480.

Han S, Liu B C, Shi C X, et al. 2020. Evaluation of CLDAS and GLDAS datasets for near-surface air temperature over major land areas of China. Sustainability, 12(10): 4311, doi: 10.3390/su12104311.

Han X, Li X, Hendricks Franssen H J, et al. 2012. Spatial horizontal correlation characteristics in the land data assimilation of soil moisture. Hydrology and Earth System Sciences, 16(5): 1349–1363.

Hu F M, Wei Z S, Zhang W, et al. 2020. A spatial downscaling method for SMAP soil moisture through visible and shortwave-infrared remote sensing data. Journal of Hydrology, 590(12): 125360, doi: 10.1016/j.jhydrol.2020.125360.

Huang X R, Bao A M, Guo H, et al. 2022. Spatiotemporal changes of typical glaciers and their responses to climate change in Xinjiang, Northwest China. Journal of Arid Land, 14(5): 502–520.

Jung C, Lee Y, Cho Y, et al. 2017. A study of spatial soil moisture estimation using a multiple linear regression model and MODIS land surface temperature data corrected by conditional merging. Remote Sensing, 9(8): 870, doi: 10.3390/rs9080870.

Kang J, Jin R, Li X, et al. 2018. Spatial upscaling of sparse soil moisture observations based on ridge regression. Remote Sensing, 10(2): 192, doi: 10.3390/rs10020192.

Klaus S, Wouter D, Richard D. 2010. Triple collocation-a new tool to determine the error structure of global soil moisture products. In: 2010 IEEE International Geoscience and Remote Sensing Symposium, Honolulu, HI, USA, 4426–4429.

Lal P, Singh G, Das N N, et al. 2022. Assessment of ERA5-land volumetric soil water layer product using *in situ* and SMAP soil moisture observations. Geoscience and Remote Sensing Letters, 19: 2508305, doi: 10.1109/LGRS.2022.3223985.

Lal P, Shekhar A, Gharun M, et al. 2023. Spatiotemporal evolution of global long-term patterns of soil moisture. Science of the Total Environment, 867(16): 161470, doi: 10.1016/j.scitotenv.2023.161470.

Li W W, Yan D H, Weng B S, et al. 2024. Nonlinear effects of surface soil moisture changes on vegetation greenness over the Tibetan Plateau. Remote Sensing of Environment, 302(11): 113971, doi: 10.1016/j.rse.2023.113971.

Li X Y, Liu L C, Duan Z H, et al. 2013. Spatio-temporal variability in remotely sensed surface soil moisture and its relationship with precipitation and evapotranspiration during the growing season in the Loess Plateau, China. Environmental Earth Sciences, 71(4): 1809–1820.

Li Y, Piao S L, Li L Z X, et al. 2018. Divergent hydrological response to large-scale afforestation and vegetation greening in China. Science Advances, 4(5): 4182, doi: 10.1126/sciadv.aar4182.

Lin X, Huang S Z, Li J F, et al. 2023. Feedback dynamics between precipitation, temperature, and soil moisture in China and their possible driving mechanisms under a changing environment. Atmospheric Research, 294(10): 106983, doi: 10.1016/j.atmosres.2023.106983.

Liu J Y, Zhang J W, Kong D D, et al. 2021. Contributions of anthropogenic forcing to evapotranspiration changes over 1980–2020 using GLEAM and CMIP6 simulations. Journal of Geophysical Research: Atmospheres, 126(22): 35367, doi: 10.1029/ 2021jd035367.

Luo X R, Li S D, Yang W N, et al. 2023. Spatio-temporal changes in global root zone soil moisture from 1981 to 2017. Journal of Hydrology, 626(13): 130297, doi: 10.1016/j.jhydrol.2023.130297.

Ma H J, Zeng J Y, Chen N C, et al. 2019. Satellite surface soil moisture from SMAP, SMOS, AMSR2 and ESA CCI: A comprehensive assessment using global ground-based observations. Remote Sensing of Environment, 231(11): 111215, doi: 10.1016/j.rse.2019.111215.

Mann H B. 1945. Nonparametric tests against trend. Econometrica, 13(3): 245–259.

Mao T N, Wei S G, Li Q L, et al. 2022. A spatial downscaling method for remote sensing soil moisture based on random forest considering soil moisture memory and mass conservation. Remote Sensing, 14(16): 3858, doi: 10.3390/rs14163858.

McColl K A, Vogelzang J, Konings A G, et al. 2014. Extended triple collocation: Estimating errors and correlation coefficients with respect to an unknown target. Geophysical Research Letters, 41(17): 6229–6236.

McColl K A, Alemohammad S H, Akbar R, et al. 2017. The global distribution and dynamics of surface soil moisture. Nature Geoscience, 10(2): 100–104.

Meng X Y, Wang H, Chen J, et al. 2019. High-resolution simulation and validation of soil moisture in the arid region of Northwest China. Scientific Reports, 9(17): 17227, doi: 10.1038/s41598-019-52923-x.

Miao Y B, Niu J Z, Wang D, et al. 2024. Greening of China and possible vegetation effects on soil moisture. Ecological Indicators, 158(11): 111382, doi: 10.1016/j.ecolind.2023.111382.

Miralles D G, Holmes T R H, De Jeu R A M, et al. 2011. Global land-surface evaporation estimated from satellite-based observations. Hydrology and Earth System Sciences, 15(2): 453–469.

Muñoz-Sabater J, Isaksen L, Balsamo G, et al. 2012. Soil moisture analyses at ECMWF: Evaluation using global ground-based *in situ* observations. Journal of Hydrometeorology, 13(5): 1442–1460.

Muñoz-Sabater J, Dutra E, Agustí-Panareda A, et al. 2021. ERA5-Land: A state-of-the-art global reanalysis dataset for land applications. Earth System Science Data, 13(9): 4349–4383.

Njoku E G, Jackson T J, Lakshmi V, et al. 2003. Soil moisture retrieval from AMSR-E. Transactions on Geoscience and Remote Sensing, 41(2): 215–229.

Ojha N, Mahmoodi A, Mialon A, et al. 2024. Assessment of SMOS root zone soil moisture: A comparative study using SMAP, ERA5, and GLDAS. IEEE Access, 12: 76121–76132.

Owe M, de Jeu R Holmes T. 2008. Multisensor historical climatology of satellite-derived global land surface moisture. Journal of Geophysical Research: Earth Surface, 113(F1): F01002, doi: 10.1029/2007jf000769.

Peng J, Loew A. 2017. Recent advances in soil moisture estimation from remote sensing. Water, 9(7): 530, doi: 10.3390/w9070530.

Piao S L, Wang X H, Park T, et al. 2019. Characteristics, drivers and feedbacks of global greening. Nature Reviews Earth & Environment, 1(1): 14–27.

Rahmani A, Golian S, Brocca L. 2016. Multiyear monitoring of soil moisture over Iran through satellite and reanalysis soil moisture products. International Journal of Applied Earth Observation and Geoinformation, 48: 85–95.

Rodell M, Houser P R, Jambor U, et al. 2004. The global land data assimilation system. Bulletin of the American Meteorological Society, 85(3): 381–394.

Sen P K. 1968. Estimates of the regression coefficient based on Kendall's Tau. Journal of the American Statistical Association, 63(324): 1379–1389.

Seneviratne S I, Corti T, Davin E L, et al. 2010. Investigating soil moisture–climate interactions in a changing climate: A review. Earth-Science Reviews, 99(3–4): 125–161.

Stoffelen A. 1998. Toward the true near-surface wind speed: Error modeling and calibration using triple collocation. Journal of Geophysical Research: Oceans, 103(C4): 7755–7766.

Su C H, Ryu D, Crow W T, et al. 2014. Beyond triple collocation: Applications to soil moisture monitoring. Journal of Geophysical Research: Atmospheres, 119(11): 6419–6439.

Tang G Q, Clark M P, Papalexiou S M, et al. 2020. Have satellite precipitation products improved over last two decades? A comprehensive comparison of GPM IMERG with nine satellite and reanalysis datasets. Remote Sensing of Environment, 240(11): 111697, doi: 10.1016/j.rse.2020.111697.

Tian J X, Zhang Z X, Zhao T B, et al. 2022. Warmer and wetter climate induced by the continual increase in atmospheric temperature and precipitable water vapor over the arid and semi-arid regions of Northwest China. Journal of Hydrology: Regional Studies, 42(10): 101151, doi: 10.1016/j.ejrh.2022.101151.

Villegas J C, Breshears D D, Zou C B, et al. 2010. Ecohydrological controls of soil evaporation in deciduous drylands: How the hierarchical effects of litter, patch and vegetation mosaic cover interact with phenology and season. Journal of Arid Environments, 74(5): 595–602.

Wagner W, Dorigo W, de Jeu R, et al. 2012. Fusion of active and passive microwave observations to create an essential climate variable data record on soil moisture. ISPRS Annals of the Photogrammetry, Remote Sensing and Spatial Information Sciences, 1(7): 315–3212.

Wang S, Fu B J, Gao G Y, et al. 2013. Responses of soil moisture in different land cover types to rainfall events in a re-vegetation catchment area of the Loess Plateau, China. CATENA, 101: 122–128.

Wang X H, Wang B T, Xu X Y, et al. 2018a. Spatial and temporal variations in surface soil moisture and vegetation cover in the Loess Plateau from 2000 to 2015. Ecological Indicators, 95: 320–330.

Wang Y Q, Shao M A, Zhu Y J, et al. 2018b. A new index to quantify dried soil layers in water-limited ecosystems: A case study on the Chinese Loess Plateau. Geoderma, 322: 1–11.

Wu W R, Geller M A, Dickinson R E. 2002. The response of soil moisture to long-term variability of precipitation. Journal of Hydrometeorology, 3(5): 604–613.

Wu X J, Shen Y P, Zhang W, et al. 2020. Fast warming has accelerated snow cover loss during spring and summer across the Northern Hemisphere over the past 52 years (1967–2018). Atmosphere, 11(7): 728, doi: 10.3390/atmos11070728.

Wu Z Y, Feng H H, He H, et al. 2021. Evaluation of soil moisture climatology and anomaly components derived from ERA5-Land and GLDAS-2.1 in China. Water Resources Management, 35(2): 629–643.

Xu L, Zheng C L, Ma Y. 2020. Variations in precipitation extremes in the arid and semi-arid regions of China. International Journal of Climatology, 41(3): 1542–1554.

Xu L, Gao G Y, Wang X F, et al. 2023. Distinguishing the effects of climate change and vegetation greening on soil moisture variability along aridity gradient in the drylands of northern China. Agricultural and Forest Meteorology, 343(10): 109786, doi: 10.1016/j.agrformet.2023.109786.

Yang L, Wei W, Chen L D, et al. 2014. Response of temporal variation of soil moisture to vegetation restoration in semi-arid Loess Plateau, China. CATENA, 115: 123–133.

Yao X L, Jiang Q, Liu Y, et al. 2021. Spatiotemporal variation of soil moisture in Northern China based on climate change initiative data. Agronomy Journal, 113(2): 774–785.

Yue S, Pilon P, Cavadias G. 2002. Power of the Mann-Kendall and Spearman's rho tests for detecting monotonic trends in hydrological series. Journal of Hydrology, 259(1–4): 254–271.

Zhang G X, Su X L, Ayantobo O O, et al. 2021. Drought monitoring and evaluation using ESA CCI and GLDAS-Noah soil moisture datasets across China. Theoretical and Applied Climatology, 144(3–4): 1407–1418.

Zhang H, Kattel G R, Wang G J, et al. 2023a. Enhanced soil moisture improves vegetation growth in an arid grassland of Inner Mongolia Autonomous Region, China. Journal of Arid Land, 15(7): 871–885.

Zhang K, Wang Q Q, Chao L J, et al. 2019. Ground observation-based analysis of soil moisture spatiotemporal variability across a humid to semi-humid transitional zone in China. Journal of Hydrology, 574: 903–914.

Zhang L M, Yang Y P, Liu Y X Y, et al. 2023b. Evaluation of long time-series soil moisture products using extended triple collocation and *in situ* measurements in China. Atmosphere, 14(9): 1351, doi: 10.3390/atmos14091351.

Zhang M Y, Cao Y, Zhang Z Y, et al. 2024. Spatiotemporal variation of land surface temperature and its driving factors in Xinjiang, China. Journal of Arid Land, 16(3): 373–395.

Zhang S L, Yang D W, Yang Y T, et al. 2018. Excessive afforestation and soil drying on China's Loess Plateau. Journal of Geophysical Research: Biogeosciences, 123(3): 923–935.

Zhao B, Mao K B, Cai Y L, et al. 2020. A combined Terra and Aqua MODIS land surface temperature and meteorological station data product for China from 2003 to 2017. Earth System Science Data, 12(4): 2555–2577.

Zhao P Q. 2021. Analysis of ecosystem pattern and driving force of Loess Plateau in Longdong. Journal of Xinyang Normal University, 34(1): 61–67. (in Chinese)

Zhao Y, Chen Y N, Wu C Y, et al. 2023. Exploring the contribution of environmental factors to evapotranspiration dynamics in the Three-River-Source region, China. Journal of Hydrology, 626(13): 130222, doi: 10.1016/j.jhydrol.2023.130222.

Zhao Y X, Shi H X. 2022. Temporal and spatial variation characteristics of soil moisture in spring in the arid regions of Northwest China in the past 60s years. Journal of Geoscience and Environment Protection, 10(12): 273–282.

Zhou S, Williams A P, Lintner B R, et al. 2021. Soil moisture–atmosphere feedbacks mitigate declining water availability in drylands. Nature Climate Change, 11(1): 38–44.

Zhu L L, Ma G Y, Zhang Y H, et al. 2022. Accelerated decline of snow cover in China from 1979 to 2018 observed from space. Science of the Total Environment, 814(15): 152491, doi: 10.1016/j.scitotenv.2021.152491.

Zhu L Y, Wang H Q, Tong C, et al. 2019. Evaluation of ESA active, passive and combined soil moisture products using upscaled ground measurements. Sensors (Basel), 19(12): 2718, doi: 10.3390/s19122718.